Acta Biomaterialia 164 (2023) 282–292

Contents lists available at ScienceDirect

Acta Biomaterialia

journal homepage: www.elsevier.com/locate/actbio

Full length article

Strain-induced collagen denaturation is rate dependent in failure of cerebral arteries

William J. Anderl[a,1], Noah Pearson[a,1], Matthew I. Converse[a], S. Michael Yu[b,c], Kenneth L. Monson[a,b,*]

[a] Department of Mechanical Engineering, University of Utah, United States
[b] Department of Biomedical Engineering, University of Utah, United States
[c] Department of Molecular Pharmaceutics, University of Utah, United States

ARTICLE INFO

Article history:
Received 29 October 2022
Revised 6 April 2023
Accepted 21 April 2023
Available online 26 April 2023

Keywords:
Collagen
Fibril
Molecular damage
Soft tissue damage
Viscoelasticity
Hyperviscoelastic-damage
Collagen hybridizing peptide
High strain rate
Cerebral artery
Traumatic brain injury

ABSTRACT

While soft tissues are commonly damaged by mechanical loading, the manifestation of this damage at the microstructural level is not fully understood. Specifically, while rate-induced stiffening has been previously observed in cerebral arteries, associated changes in microstructural damage patterns following high-rate loading are largely undefined. In this study, we stretched porcine middle cerebral arteries to failure at 0.01 and >150 s^{-1}, both axially and circumferentially, followed by probing for denatured tropocollagen using collagen hybridizing peptide (CHP). We found that collagen fibrils aligned with the loading direction experienced less denaturation following failure tests at high than low rates. Others have demonstrated similar rate dependence in tropocollagen denaturation during soft tissue failure, but this is the first study to quantify this behavior using CHP and to report it for cerebral arteries. These findings may have significant implications for traumatic brain injury and intracranial balloon angioplasty. We additionally observed possible tropocollagen denaturation in vessel layers primarily composed of fibrils transversely aligned to the loading axis. To our knowledge, this is the first observation of collagen denaturation due to transverse loading, but further research is needed to confirm this finding.

Statement of significance

Previous work shows that collagen hybridizing peptide (CHP) can be used to identify collagen molecule unfolding and denaturation in mechanically overloaded soft tissues, including the cerebral arteries. But experiments have not explored collagen damage at rates relevant to traumatic brain injury. In this work, we quantified collagen damage in cerebral arteries stretched to failure at both high and low rates. We found that the collagen molecule is less damaged at high than at low rates, suggesting that damage mechanisms of either the collagen molecule or other elements of the collagen superstructure are rate dependent. This work implies that arteries failed at high rates, such as in traumatic brain injury, will have different molecular-level damage patterns than arteries failed at low rates. Consequently, improved understanding of damage characteristics may be expanded in the future to better inform clinically relevant cases of collagen damage such as angioplasty and injury healing.

1. Introduction

1.1. Constituent damage in arteries

Cerebral arteries play a critical role in sustaining life, as they are responsible for continuously distributing nutrients to the brain. While arteries are highly durable tissue, they are commonly damaged through trauma, such as traumatic brain injury (TBI) [1,2], as well as by surgical procedures such as angioplasty [3]. Vessel injury has been widely studied and includes investigations of gross tissue failure and hemorrhage [4,5], cellular dysfunction [6], and injury to the extracellular matrix (ECM) [7–9]. Furthermore, persistent changes to the mechanical response of arteries subsequent to overstretch have been reported following both circumferential and axial loading [10–12]. Much of this research aims to associate ECM damage with changes to the mechanical response of the tissue [13–17], and to thus allow a better understanding of the

[1] Co-first author.
* Corresponding author at: 1495 E. 100 S., MEK 1550, Salt Lake City, UT, USA 84112.
E-mail address: ken.monson@mech.utah.edu (K.L. Monson).

https://doi.org/10.1016/j.actbio.2023.04.032
1742-7061/

implications of injury, angioplasty, and even remodeling of aneurysms [4,18].

1.2. Rate dependence and microstructure

Many soft tissues, including arteries, are strain-rate sensitive. This rate sensitivity implies that when the material is deformed sufficiently slowly, the tissue's internal microstructure can freely reorganize to achieve the lowest internal energy configuration for the current deformation. The material thus constantly dissipates energy and only stores the absolute minimum energy at truly quasi-static strain rates. However, at high strain rates, the molecules cannot reorganize quickly enough to reach the minimum energy state for the current stretch. As stiffness is the second derivative of this strain energy with respect to strain, the inability of these tissues to reorganize is manifest as rate-dependent stiffening, such that higher strain rates produce higher stresses at a given level of stretch. There is some disagreement among researchers regarding the rate dependence of arteries [19–26], perhaps due to different animal species and vessel types.

Given the observed rate-induced changes to microstructural energy dissipation in arteries, we anticipate an associated change in microstructural damage patterns, similar to that discussed in the broader soft tissue literature. Willet et al. observed a rate-dependent change in the binding rate of trypsin in tendon [27] that they attributed to the imposed strain rate being too high for intermolecular sliding, limiting the number of sites available for proteolysis. Continuing this work, Chambers et al. identified a strain rate dependence of ultrastructural damage in bovine digital tendons between 1 and 10% s^{-1} [28]. As arteries are often deformed to failure and bleed in TBI, we can assume that other intact vessels are also overstretched, though not to the point of failure. We have previously observed molecular-level collagen denaturation in cerebral arteries subjected to low-rate loading [10], but damage patterns occurring at the high-rate deformations of TBI have not been defined.

1.3. Probing collagen structure

As discussed in detail elsewhere [2], healthy cerebral arteries have three layers: intima, media, and adventitia. The intima is composed of a layer of endothelial cells adhered to a thin basement membrane and is generally not considered to be mechanically relevant. The intima is separated from the media by the internal elastic lamina (IEL); this structure is the primary site of elastin in cerebral arteries. The media is made up of two helically opposed collagen fiber families that are largely circumferentially oriented. The media also contains smooth muscle cells that control dilation necessary to regulate the flow of blood in the brain. The adventitia largely consists of axially oriented fibers with a higher degree of dispersion than the medial fibers.

Fibrous collagen has a prominent structural hierarchy in fully matured tissues. Collagen fibers are large, optically resolved structures made up of many so-called collagen fibrils primarily bound together by proteoglycan bridges [29]. These fibrils, in turn, are made of bundles of tropocollagens, also known as collagen molecules, tightly packed together with short chemical crosslinks [30]. The tropocollagen molecule is itself a super-secondary protein structure comprised of three polypeptide strands, called alpha chains, wrapped into a triple helix [31].

A recently developed collagen-hybridizing peptide (CHP) leverages a synthetic alpha chain imitation to enable reliable quantification of tropocollagen unwinding and denaturation [32–34]. CHP has lately been applied to identify mechanically induced damage to the tropocollagen matrix following overstretch of blood vessels and tendons [10,34-38]. Furthermore, the amount of tropocollagen damage has been shown to correlate with both degree of overstretch [10,38] and number of fatigue cycles [36].

1.4. Study goals

To investigate the influence of strain rate on mechanical damage to tropocollagen, we stretched cerebral arteries to failure at low (0.01 s^{-1}) and high (>150 s^{-1}) rates, in both the axial and circumferential directions. We then probed the failed vessels for tropocollagen denaturation using CHP.

2. Materials and methods

2.1. Overview

Göttingen minipig middle cerebral arteries (MCAs) were pulled to failure at either low rate (0.01 s^{-1}) or at high rate (>150 s^{-1}), and in either the axial or circumferential direction. The low rate was arbitrarily selected as a value that would still allow a reasonable test completion time, and the high rate was chosen to be consistent with severe blast TBI [39,40]. Following failure, vessels were stained with fluorescent CHP, mounted onto slides, and imaged using confocal microscopy. The same samples were then digested with Proteinase K, and CHP fluorescence of the resulting liquid was quantified. Fluorescence relative to controls was evaluated and compared between groups to determine the effect of strain rate and loading direction on collagen damage. The axial samples were randomly selected from a set of samples used for a previous publication on mechanical response [26].

2.2. Tissue preparation

Göttingen minipigs were euthanized by Beuthanasia overdose following a protocol approved by the University of Utah Animal Care and Use Committee. The brain was removed from the head and placed in calcium-free phosphate-buffered saline (PBS). MCAs were then resected, the pia-arachnoid complex was removed, and any side branches were ligated. Multiple test samples were harvested from a single MCA. Arteries were stored in PBS at 4 °C until testing. All tests were performed within 48 h of death. Dissected control sections of MCAs were maintained from each animal for use as a baseline reading of CHP.

2.3. Apparatus

Tests were conducted as previously described by Converse et al. [10], except that all vessels were stretched to failure, some at high rates. Briefly, for axial tests, intact vessels approximately 5 mm long were cannulated onto size-matched needles submerged in a calcium-free PBS bath. The arteries were secured to the cannulas with 6–0 suture, and cyanoacrylate was applied distally to further secure samples to the needles. A voice coil actuator (AVM60–25, Motion Control Products, Bournemouth, UK) provided low-rate axial displacements, and a syringe pump was used to maintain pressure. Circumferentially stretched samples were cut into rings approximately 1 mm in length and penetrated with parallel needles, similar to typical wire myography. A digital camera (PL-A741, Pixelink, Rochester, NY) recorded specimen motion to allow determination of strains.

High-rate tests in both directions utilized a drop tower described by Bell et al. [25]; the voice coil was replaced with the drop tower where a steel ball was dropped into a catchment that transferred momentum to the fixture on one end of the artery via a steel cable. Additionally, the low frame-rate camera was replaced by a high frame-rate camera (Phantom Miro EX4, Vision Research, Perth, Australia) to capture the high-rate deformations at 25 kHz.

2.4. Mechanical test procedure

In axial tests, arteries were preconditioned by oscillating luminal pressure from 50 to 150 mmHg five times at a given axial stretch (defined as the ratio of the current length to the length at which the vessel carried no axial load in an unpressurized configuration). Axial stretch was incrementally increased from 1.0 to the axial in vivo stretch, the configuration where no change in axial force was detected during a pressure cycle as noted by Weizsacker et al. [41]. One additional preconditioning cycle was then conducted at an axial stretch of 1.10 times the in vivo stretch. Following preconditioning, arteries were set to a physiologic luminal pressure (80 or 120 mmHg), axially buckled, and then pulled axially to failure at either a low rate (0.01 s^{-1}) or at a high rate (>150 s^{-1}). The bath was drained immediately prior to the high-rate failure ramps. Samples were exposed to air for less than 30 s prior to failure.

For circumferential tests, circumferential stretch was defined as the ratio of the current circumference to the reference circumference. The current circumference was defined as

$$c = 2x_n + \pi\,(D_n + H) \tag{1}$$

where x_n is the distance between the center of the needles, D_n is the diameter of the needles, and H is the reference wall thickness of the ring. The reference circumference of the sample was optically determined by imaging each side of the ring prior to testing and averaging the identified circumferences. Samples were mounted onto the tester, stretched to 1.10 times the in vivo stretch, and allowed to stress-relax for five minutes to precondition the tissue. The in vivo circumferential stretch was approximated as the average circumferential stretch observed during preconditioning of all axial samples when pressurized to the mean physiologic pressure of 100 mmHg and axially extended to in vivo stretch. Rings were unloaded and then circumferentially stretched to failure at either a low rate (0.01 s^{-1}) or at a high rate (>150 s^{-1}). The maximum strain rate in the circumferential direction was chosen to be the same as in the axial direction because deformation rates in the circumferential direction of arteries during TBI are unknown.

2.5. Staining

Immediately following failure, samples were returned to a PBS bath and refrigerated until staining, as previously described [10]. Briefly, a solution of 20 µM F-CHP (fluorophore tagged CHP; 3Helix #FLU300, Salt Lake City) was prepared in PBS. This solution was heated to 80 °C for 10 min and then cooled in an ice bath for 2 min. The tested arteries and associated controls were then each placed in 100 µL of the F-CHP solution and incubated at 4 °C for at least 16 h. Following incubation, each vessel underwent three rinsing cycles in which they were repeatedly placed in a fresh PBS solution for 30 min with gentle agitation. After the final rinse, vessels were cut open longitudinally and laid flat, intima down, on glass slides using a mounting medium of Fluoromount (Fluoromount G; Southern Biotech).

2.6. Confocal microscopy and image analysis

Each vessel was imaged using a confocal microscope with a 10X objective (Fluoview FV1000, Olympus), excited with the 488 nm laser channel (F-CHP emission is 512 nm). Several fields of view (512 × 512 pixels) were used to capture the entire vessel area at z-axis increments of 2 µm through the vessel wall for a complete digital capture of the vessel volume. Following image acquisition, a custom MATLAB (2021b, MathWorks) code was used to stitch images together such that the vessel could be analyzed in entirety.

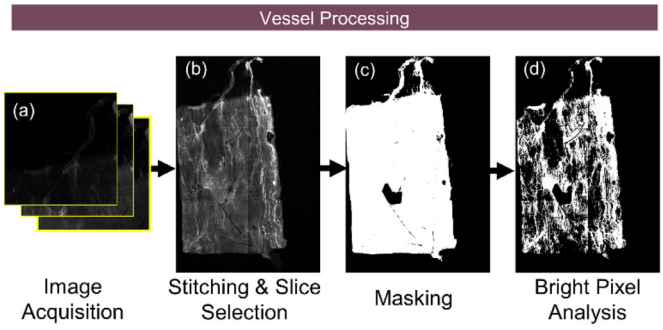

Fig. 1. Flowchart of image acquisition and processing. Images (512 × 512 pixels) were captured and stitched, followed by either manual or automated approaches to evaluate CHP attachment. Bright pixels (d) are reported as a percentage of unmasked area (c).

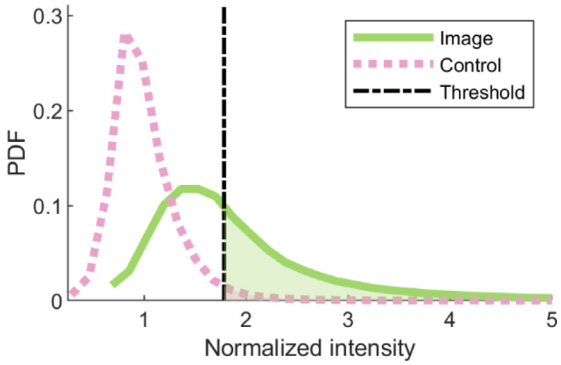

Fig. 2. Image characteristics used during vessel processing for a representative sample. The number of pixels brighter than two standard deviations above the mean of the control sample, as shown by the shaded region of the probability density function (PDF), was used to determine percent bright pixels.

Vessels were analyzed with a semi-manual approach (Fig. 1). A single slice from each layer (media and adventitia) of the artery was used to quantify the CHP binding of the entire layer. Collagen fiber direction was used to identify which layer each image slice belonged to; that is, adventitial slices were selected as those in which the preponderance of visible collagen fibers were oriented along the axis of the vessel, and medial slices were selected for a predominant circumferential fiber orientation. The brightest slice within the identified layers was selected as the representative slice. The deepest selected slice was approximately 40 µm deep in the tissue. Following stitching and slice selection, a digital mask was created to remove the image background, non-biological artifacts (i.e. sutures and dust), and confounding features such as areas of bunched tissue. Occasionally, image capture areas overlapped during microscopy, leading to double exposure of some tissue; these were also manually identified by noting areas of obvious photobleaching and removed. The remaining (unmasked) vessel area was evaluated for attached CHP following a strategy similar to one previously developed [10]. Briefly, each sample, including controls, was normalized by the mean intensity value of its masked control (or, in the case of a control, normalized by its own mean). A threshold was defined at two standard deviations above the mean of the normalized control image brightness (Fig. 2). The percent of pixels in the normalized sample image brighter than this threshold (two standard deviations above the control mean) was determined and used as the final metric of damage.

2.7. Proteinase K assay

To explore high throughput options, samples from the axially stretched group were removed from slides and placed in 100 µL

of 1 mg/mL Proteinase K (Sigma Aldrich, P2308) at 60 °C for 24 h after confocal imaging; we found that exposure for three hours (as suggested by Lin for tendon [42]) did not appear to adequately homogenize these cerebral vessels, potentially due to additional structural constituents in blood vessels. After enzymatic homogenization, the volume was split into two 50 µL duplicates, and fluorescence was quantified using a microplate reader (SpectraMax Gemini XPS) set to an excitation wavelength of 485 nm and an emission wavelength of 525 nm, as outlined by Lin et al.

Multiple techniques were evaluated for normalizing total fluorescence. The first technique used was simply normalizing by the two-dimensional area of the vessel, as obtained during confocal microscopy. The second normalization technique was dry sample weight measured using a microbalance (UMX2 ultra-microbalance, Mettler Toledo). The final technique was a hydroxyproline assay (Sigma-Aldrich MAK008), performed to quantify the amount of collagen in the sample by virtue of the amount of hydroxyproline (an amino acid largely restricted to collagen) [43]. In brief, the oxidized hydroxyproline in a hydrolyzed solution of the digested samples (after microplate reading of CHP fluorescence) was reacted with 4-(dimethylamino)benzaldehyde to produce a colorimetric solution. The absorbance was read at 561 nm by the microplate reader. The absorbance, proportional to hydroxyproline content, was compared to a standard curve to calculate the concentration of hydroxyproline in the solution, and by extension, the amount of collagen in the sample.

2.8. Statistical analysis

Student's *t*-test was used to compare the low-rate and high-rate groups for each test type (i.e., the effect of rate was separately evaluated in both the adventitia and media in both axially and circumferentially stretched samples). Because results from different layers and test directions were categorically different, layer and test direction were not evaluated as variables.

3. Results

As in our previous work, experiments here produced collagen molecule damage in fibers aligned with the direction of loading. However, these experiments also revealed CHP binding in vessel layers where the predominant fiber direction is transverse to the direction of loading (e.g., medial damage resulting from axial loading). As a result, we differentiate between damage observed in fibers aligned with and transverse to the direction of loading in the Results and Discussion.

3.1. Rate dependence of tropocollagen damage in fibers aligned with loading direction

Aligned loading resulted in different extents of tropocollagen denaturation between the low-rate and high-rate groups as identified by confocal microscopy. Axial samples pulled at low rate showed visually apparent areas of axially oriented fibrous damage in the adventitia (Fig. 3), similar to that reported in our previous work [10]. Generally, vessels pulled at high rates showed little fibrous damage. This visually apparent difference between rate groups was confirmed statistically (Figure 4; $p = 0.025$, manual masking). Although high-rate samples displayed significantly less denaturation than low-rate vessels, CHP staining was still substantially greater than that found in controls.

As with the adventitia of axially stretched specimens, the media of vessels failed circumferentially showed generally increased

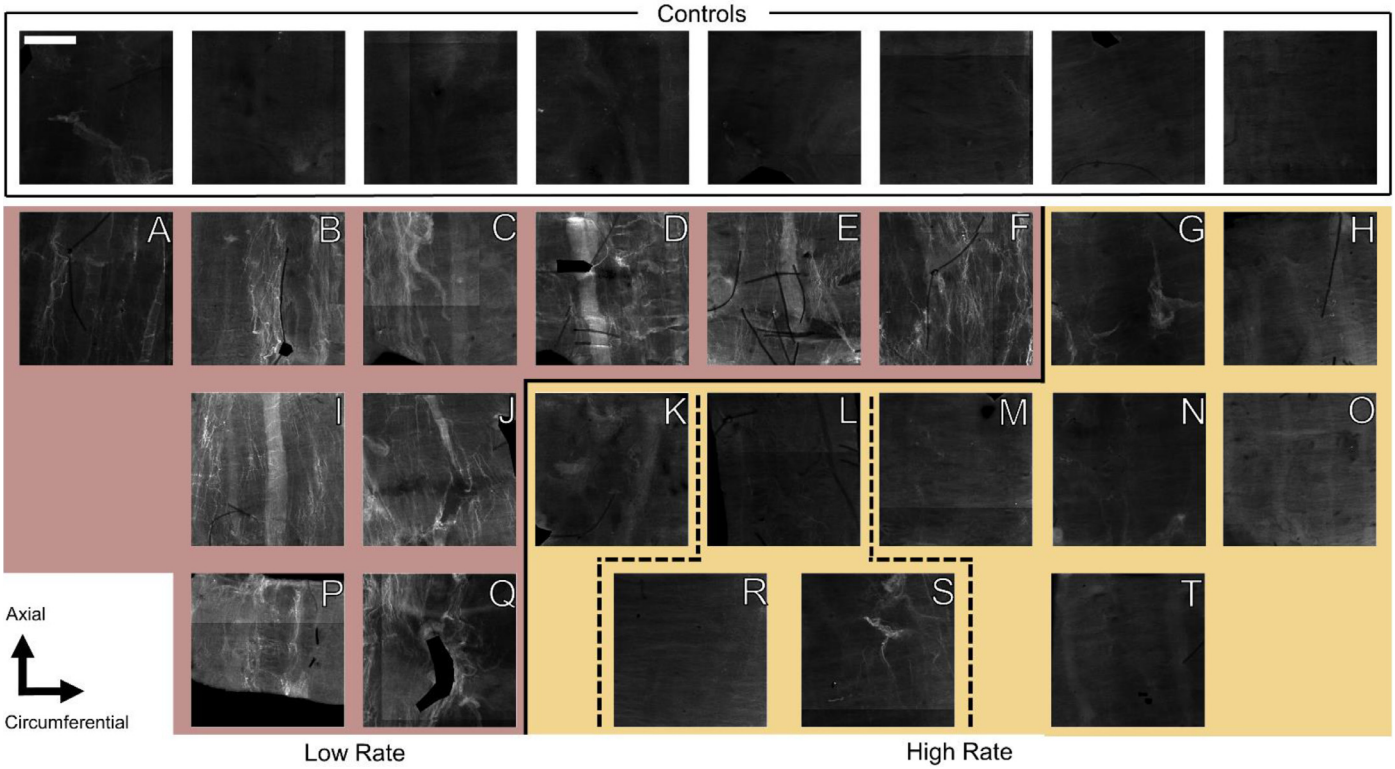

Fig. 3. Adventitial tropocollagen denaturation in vessels stretched axially at low rate (left) and high rates (right). A single representative image was selected from each vessel to demonstrate observed differences in damage patterns. The first row consists of controls; corresponding damaged vessels are displayed vertically beneath each control. Multiple test samples were collected from each MCA leading to multiple samples per control. A strong trend of rate dependence was observed, with vessels stretched at low rate exhibiting consistently more CHP attachment than high-rate counterparts. All images shown were manually masked and normalized by average control brightness to simplify visual comparison. Note that samples R and S are in the same group as E and L. Scale bar is 300 µm.

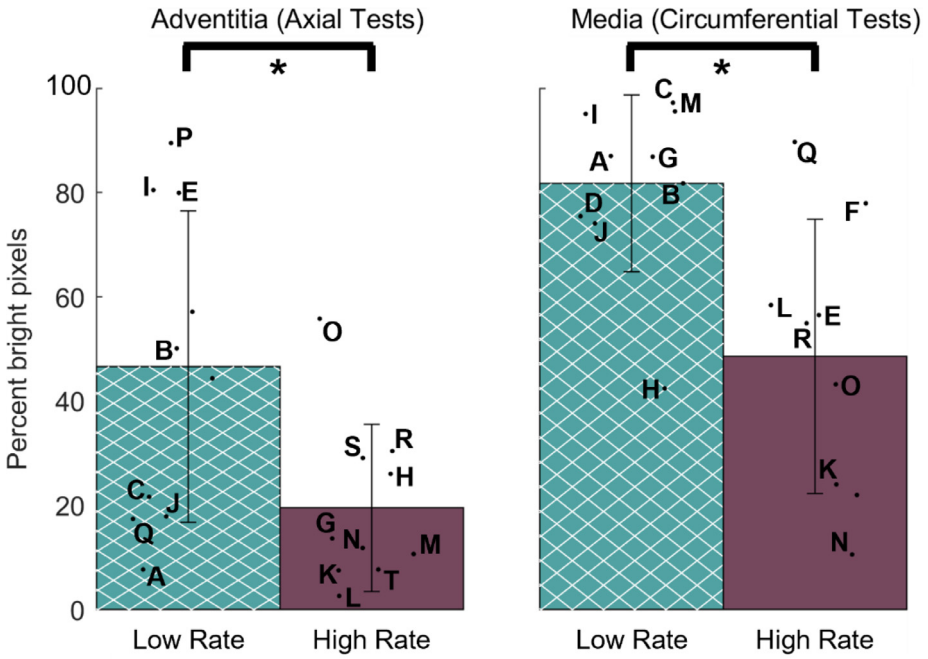

Fig. 4. Medial tropocollagen denaturation in vessels stretched circumferentially at low rate and high rate. Circumferentially damaged vessels exhibited a more diffuse brightness pattern than those stretched axially, but dependence on rate persisted. All images shown were manually masked and normalized by average control brightness to simplify visual comparison. Scale bar is 300 μm.

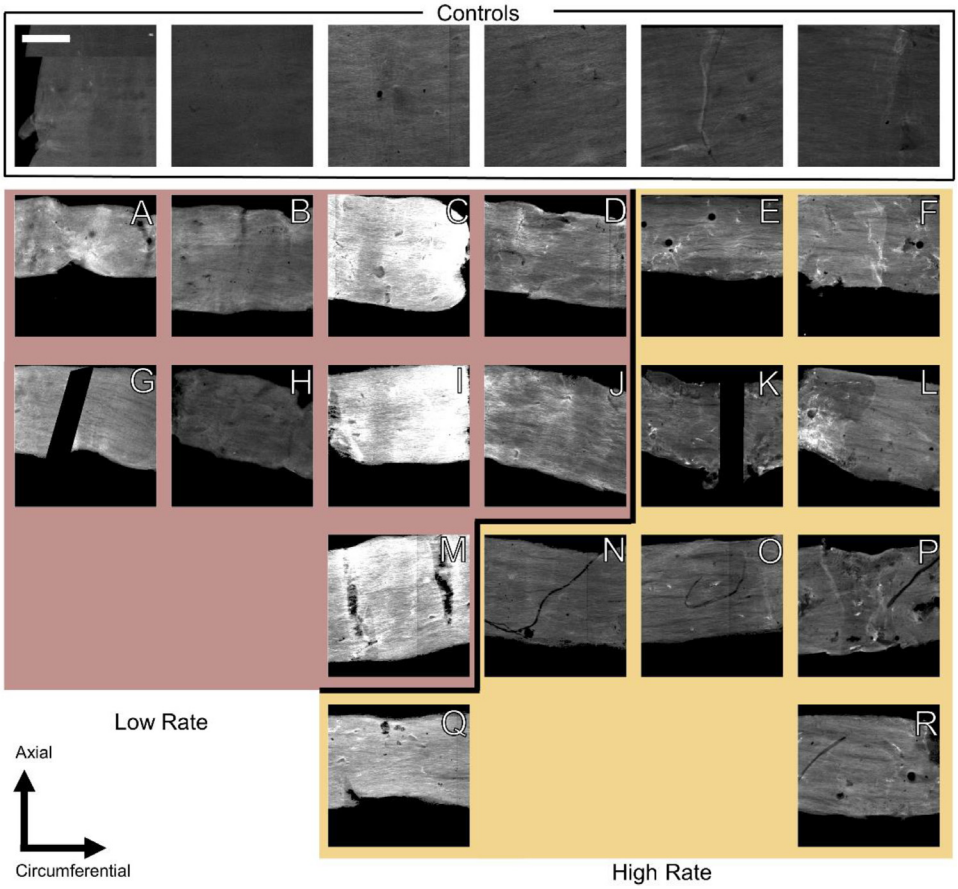

Fig. 5. Mean and standard deviation of collagen denaturation (percent bright pixels) as a function of loading rate for collagen-aligned deformation. Results for both axial (adventitia damage) and circumferential (medial damage) tests are shown. Both manual and automatic quantification results are also presented. Adventitial tropocollagen (left) is delaminated much more readily in samples axially failed at low rate than in axial samples failed at high strain-rate, as quantified by the amount of bound CHP observed with a confocal microscope. Rate dependence in aligned collagen is maintained in circumferentially failed vessels as observed by CHP expression binding in the media (right). For reference, the undeformed control samples all have 2.5% bright pixels on this scale given our methods. Letters identify quantified values for individual samples labeled in Figs. 3 and 4.

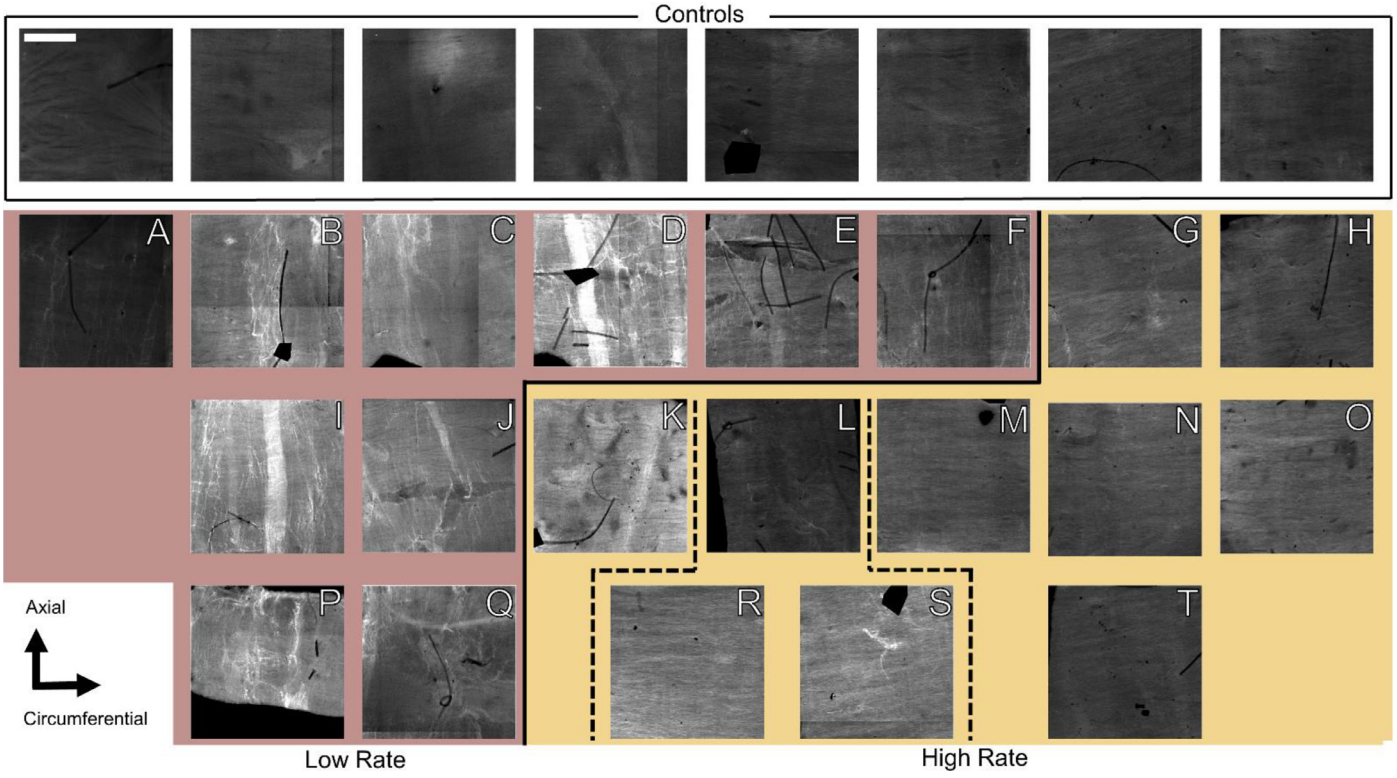

Fig. 6. Representative images of medial slices in axially stretched vessels (i.e., loading direction transverse to fiber direction). Out-of-focus light is apparent in some of the low-rate samples (for example, compare samples B and I here with B and I in Fig. 3); however, the lack of out-of-focus light in the high-rate vessels is suggestive that the detected damage is due to transverse loading, alleviating concerns that signal from the damaged adventitia leads to our conclusion of transverse damage. All images shown were manually masked and normalized by average control brightness to simplify visual comparison. Scale bar 300 μm.

Table 1
CHP quantification and *p*-values for each combination of test type and analysis layer.

	Percent bright pixels (mean ± std)		
	Low Rate	High Rate	*p*-values
Axial - Adventitia	46.6 ± 29.9	19.6 ± 16.0	0.025
Circ. - Media	81.7 ± 17.0	48.6 ± 26.3	0.007
Axial - Media	43.4 ± 25.0	36.9 ± 36.5	0.646
Circ. - Adventitia	36.1 ± 25.5	28.5 ± 15.6	0.459

denaturation at low rates compared to high rates (Fig. 5). As previously reported [10], circumferential stretch typically produced an increase in general brightness of the media in contrast to bright, individual fibers, as typical in axial stretch. Rate dependence in the media was further confirmed statistically (Figure 4; $p = 0.007$).

3.2. Evidence of tropocollagen damage in fibers transverse to the loading direction

In addition to damage seen in load-aligned fibers, increased brightness was unexpectedly observed in layers containing transversely oriented fibers, most notably in the media of axially stretched vessels (Fig. 6). Increased brightness of adventitial fibers in circumferential tests was also apparent for some cases (Fig. 7). In both cases, this damage generally appeared less distinct than that seen in aligned fibers. This increased brightness in layers with transversely oriented fibers did not appear to be dependent on strain rate, visually or statistically (Fig. 8, Table 1).

3.3. Failure mechanics

Axial failure stretch was not statistically different ($p > 0.05$) between the low- and high-rate groups in this data set, with failure stretch values of 1.52 ± 0.11 (mean ± std) for the low-rate and 1.50 ± 0.10 for the high-rate group. The axial failure stress values were similarly not significantly different between the low- and high-rate groups, with a failure stress of 5.07 ± 2.12 MPa for the low-rate group and 6.51 ± 2.84 MPa for the high-rate group. Circumferential failure stretch was significantly different ($p = 0.003$) with failure stretch values of 2.94 ± 0.17 and 2.63 ± 0.19 for the low-rate and high-rate groups, respectively. The failure stress values were also significantly different ($p < 0.001$) with a failure stress of 3.48 ± 1.77 for the low-rate group and 7.30 ± 1.37 for the high-rate group.

3.4. Enzymatic quantification

Among the three normalization methods evaluated for enzymatic digestion, two-dimensional area was found to be closely related to both vessel weight (correlation coefficient = 0.96, $n = 12$) and the hydroxyproline assay (correlation coefficient = 0.98, $n = 14$), suggesting any one of the three is reasonable to use for normalization. All presented digestion results were thus normalized by two-dimensional area. Regardless of normalization technique, and in contrast to local analysis of single layers by microscopy, global enzymatic digestion suggested no significant differences between either group of damaged vessels and their corresponding controls or between rates.

4. Discussion

The primary objective of this research was to evaluate the rate dependence of molecular-level collagen denaturation in cerebral arteries stretched to failure. Results show significantly less collagen denaturation at high rates in aligned fibers, despite all samples being pulled to structural failure. Additionally, possible evidence of

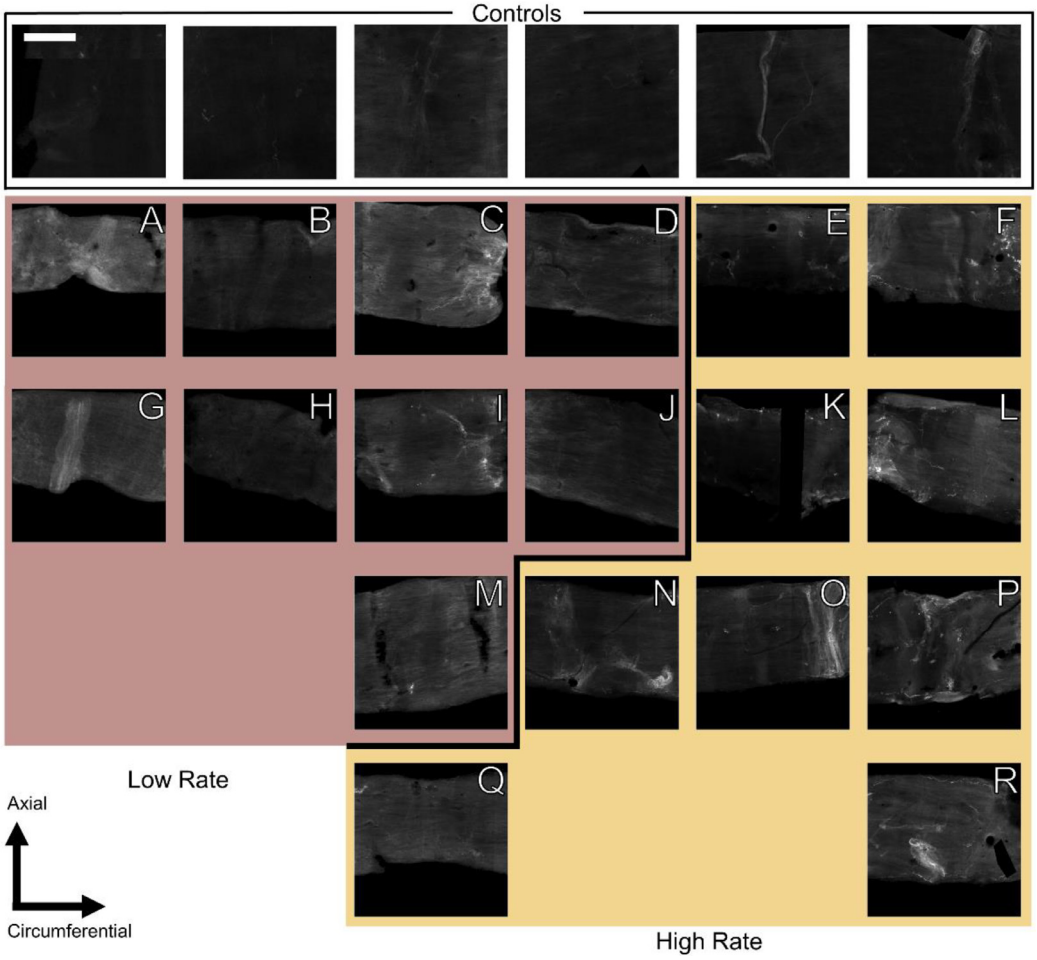

Fig. 7. Representative images of adventitial slices in circumferentially stretched vessels. Most vessels, both low and high rate, are absent of oriented fibrous damage characteristic of axially stretched samples. All images shown were manually masked and normalized by average control brightness to simplify visual comparison. Scale bar is 300 μm.

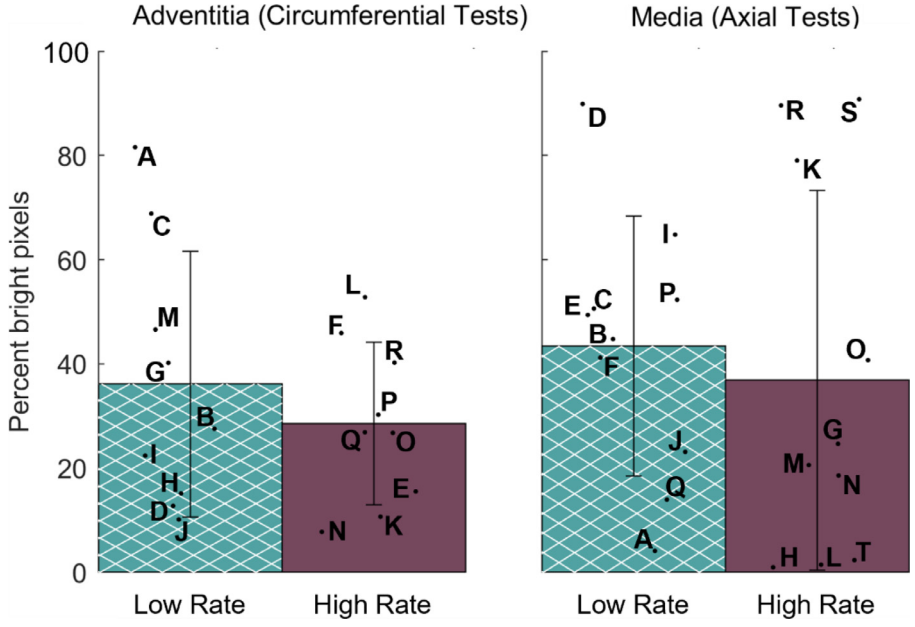

Fig. 8. Mean and standard deviation of collagen denaturation (percent bright pixels) in fibers transverse to the direction of loading, as a function of loading direction and rate. Results are summarized for medial and adventitial collagen following axial and circumferential tests, respectively. Both manual and automatic methods are shown. In both vessel layers, denaturation of transversely loaded tropocollagen is apparently unaffected by strain-rate in most comparisons.

denaturation in transversely oriented fibers was observed but was not rate dependent.

4.1. Aligned collagen

Our results show that tropocollagen denaturation is strongly dependent on rate in failure tests of cerebral arteries. While not previously observed in arteries, several researchers have reported similar results in tendon. Willet et al. failed bovine tail tendon at either 0.01 or 10 s^{-1} prior to acetyltrypsin and α-chemotrypsin proteolysis [27]. They found a statistically higher degree of tropocollagen disruption in the low-rate group than in the high-rate group in their study and subsequently reinforced the significance of rate dependence in experiments using differential scanning calorimetry [44]. Chambers et al. similarly failed bovine extensor and flexor tendons at either 1 or 10% s^{-1} and imaged the fibrils with scanning electron microscopy (SEM). While damage developed differently in the two tendon types due to cross-linking differences, results demonstrated a general decrease in tropocollagen damage with increasing rate, including no apparent collagen disruption in flexor tendons at the highest rate [28]. Although not involving tests to failure, Zitnay et al. quantified tropocollagen damage as a function of rate in cyclic fatigue experiments of rat tail tendons [37]. Using CHP, they found less tropocollagen damage per cycle at high (40% s^{-1}) than low (0.4% s^{-1}) rates.

Mechanisms governing collagen damage observed in failure of soft tissues are of interest in ongoing research. For example, the models of Zitnay et al. showed that tropocollagen unfolding is rate dependent, with weaker hydrogen bonds dominating the low-rate response and stronger covalent bonds controlling the high-rate response [36]. While it seems logical to apply these models to our findings, the larger dataset from which our axial tests here were drawn showed a statistically significant reduction of failure stretch with rate [26]. Because other work from our lab showed that the threshold for collagen denaturation is relatively high in low-rate tests of cerebral arteries [10], it is possible that this rate-induced reduction in failure stretch resulted in the collagen fibers not achieving a high enough stretch to induce tropocollagen denaturation. However, the subset evaluated here did not have different failure stretch (or stress) values for the two rates, supporting research by others indicating that rate directly affects the molecular-level failure mechanism. We note that the circumferential tests, in contrast, did show rate dependent failure stretch, leaving open the possibility that differences in stretch contributed to those results, but, based on the axial tests, we feel confident in concluding that collagen denaturation is rate dependent in arteries. This conclusion is consistent with the transition from longitudinally distributed damage to localized point failure (and non-affine deformations) with increasing strain rates observed by Chambers et al. [28], and, interestingly, with the previously reported lack of CHP binding at locations of tissue cut with scissors [10,34], where tropocollagen molecules were torn apart with little relative sliding between alpha chains at high rates.

Another possible explanation for the observed reduction in tropocollagen denaturation at high rates is that other components of the collagen hierarchy are rate dependent and fail before tropocollagen. Several groups have speculated about this question. One idea is that inter-fibrillar proteoglycans viscously slide relative to each other and that the onset of damage occurs when proteoglycan overlap decreases beyond a critical level [45,46], such that the fibril arrangement within the fiber is plastically changed. While Puxkandl et al. reported an increase in the ratio of fibril to bulk tissue elongation between 0.001 and 0.1% s^{-1} in synchrotron X-ray diffraction of rat-rail tendon [47], this observed increase in fibril strain with rate is inconsistent with more recent experiments that show rate-stiffening in isolated collagen fibrils [48]. Further, Bonner et al. performed experiments similar to those of Puxkandl et al. at higher rates (0.001–0.05 s^{-1}), in human lateral collateral ligaments, and found that increasing strain rate reduced fibril strain by a factor of approximately three at high strain [49]. These latter findings appear to agree with the here-observed reduction in tropocollagen denaturation at high rates, and suggest that strain is accumulating in the interfibrillar matrix. Bonner et al. proposed a damage mechanism wherein the interfibrillar matrix is debonded from the collagen fibrils at higher strain rates. Matrix debonding could explain our findings and would not negate a previous model of proteoglycan slipping [46], nor our observations of tropocollagen denaturation, at lower strain rates.

Our present experiment was designed to evaluate the difference between extremes of the rate spectrum expected in vivo for cerebral arteries; that is, low rates such as those experienced by angioplasty and high rates such as those expected in TBI. A limitation of this choice is that it necessitated different methods to drive the deformations. We considered the effect that wave propagation originating from the drop tower would have on the tissue response. At the current length scale, the wave speed in the principle direction is three orders of magnitude higher than the applied deformation rates, mitigating concerns about the effects of wave propagation on tissue response.

The presently reported circumferential failure stretches should only be used as a relative comparator between the low-rate and high-rate tests. Identification of the current circumference was complicated by non-homogeneous deformations around the needles and relative compliance of the needles leading to unreasonably large stretch values. But we are confident that the relative differences identified are still qualitatively accurate.

4.2. Transverse collagen

To our knowledge, this is the first study to observe possible tropocollagen denaturation in fibers oriented transverse to the direction of loading. While it is clear that the media is loaded in axial tests to failure, it is not obvious that the collagen fibers would be damaged, as they are not loaded in the fiber direction; for example, transverse loading of a single-fiber-family composite material typically results in failure of the matrix while the fibers are left intact. Because examining transverse fibers was not a focus of this study, we were initially surprised by these findings and had concerns that mounting or preconditioning was responsible for the increased CHP binding. To investigate this, we subjected a small number of samples to just the mounting and removal procedures ($n = 4$), as well as to mounting, preconditioning, and removal ($n = 3$). While these sample sizes are too small to draw firm conclusions, negligible levels of CHP binding were observed (an average of 0.07% bright pixels), suggesting that this is a real phenomenon that warrants further study.

The mechanism of this transverse damage is unclear. Collagen fibers in arteries are not perfectly aligned with the axial and circumferential directions, but are, rather, distributed around a slightly offset angle. As a deformation is applied, these fibers rotate toward the direction of loading. Canham et al. found the most extreme medial fibers to be a mean of only 1.5° offset from the circumferential direction in human MCAs [50]. Wicker et al., on the other hand, found the adventitial fibers of rabbit basilar arteries to be offset by a mean of 20.2° in samples pressurized to 80 mmHg [51]. The fiber stretch resulting from a deformation can be calculated as $\lambda_{fiber} = \sqrt{I_4}$ where the invariant $I_4 = C : a_0 \otimes a_0$ is the double contraction of C, the right Cauchy-Green tensor, and a structure tensor created by the dyad of the in-plane reference fiber direction $a_0 = [\ \cos(\theta) \quad \sin(\theta) \quad 0\ ]^T$ with itself. When evaluated with conservative reference medial and adventitial fiber directions of $\theta_{media} = 15^\circ$ and $\theta_{adventitia} = 30^\circ$ (the most extreme me-

dial and adventitial fiber directions found in Fig. 7 of Wicker et al. [51]), we find a maximum medial fiber stretch of 1.06 for our most extreme axial test and a maximum adventitial stretch of 1.60 for the circumferential tests. The average fiber directions (from the mean fiber directions listed above) lead to mean transverse fiber stretches of 1.00 and 1.28 for the medial and adventitial sheets, respectively. We thus believe the observed denaturation in the transverse sheet (media) in axial tests are highly unlikely to be a result of fiber reorientation, and that a vast majority of the fibers in the transverse sheet (adventitia) in circumferential tests do not experience high enough fiber stretches to denature.

Another consideration is the 3-D organization of collagen fibrils within a fiber. While fibrils are generally aligned with the fiber direction, some align transverse to the fiber direction at times [52]. These laterally oriented fibrils may become overstretched during transverse loading of the fiber. Such loading may also occur in crimped collagen fibers. Alternatively, Converse et al. [10] noted that fluorescence from CHP can illuminate adjacent vessel layers and lead to incorrect identification of damage there. Here, we believe that damage in transversely loaded fibers is not an imaging artifact because the signal pattern does not match that seen in load-aligned layers. All things considered, it seems reasonable that tropocollagen could also be pulled apart in the transverse direction, much like a string being separated transversely into its separate fibers. In this case, there may be less sliding between the alpha chains than in aligned fiber deformations, but binding sites would still be opened up to allow for CHP attachment.

Interestingly, we've previously demonstrated transverse softening in cerebral arteries [53], where axial overstretch induced circumferential softening. We reasoned that this was a natural consequence of damage in one direction of a biaxially loaded structure, but observations of transverse damage here suggest that it may also contribute. In any case, these results imply that contemporary continuum damage models of collagenous tissue, where collagen damage is accumulated solely as a function of fiber stretch (i.e. [17,54,55]), may need to be re-evaluated.

It is also notable that damage to transverse fibers was not rate dependent, in contrast to that in aligned fibers. This difference may shed light on rate dependent damage distribution through the collagen hierarchy with additional research.

All points considered, the identification of tropocollagen denaturation in fibers oriented transverse to the loading direction was unexpected and should be considered tentative until it can be confirmed through additional research.

4.3. Medial vs adventitial damage

As observed by Converse et al., there are qualitative differences in spatial damage patterns between the media and adventitial layers. In general, images of circumferentially stretched vessels appear to contain more noise than axially stretched samples. The circumferentially failed vessel samples were smaller than axial specimens (2-D Area Axial: 2.58 $\pm$ 0.90 mm^2, Circumferential: 1.14 $\pm$ 0.19 mm^2). As a result, a higher percentage of overall area was characterized by catastrophic tissue damage in circumferential samples. The relatively large amount of catastrophic damage creates a particular challenge when processing vessel images for circumferential samples in which the damaged tissue may fold over on itself to produce areas of artificially high fluorescence, making layer specific differences more difficult to distinguish. Masking of such areas may further lead to a substantially decreased total area available for quantification. This global disruption of specimens combined with the decreased sample size of circumferential versus axial vessels may make a significant contribution to standard deviations in the circumferential data.

4.4. Methods evaluation

Confocal evaluation of CHP-marked damage relies heavily on the experience and decision-making of the researcher performing the analysis. Masking of image artifacts and non-biological features requires manual input, providing a potential source of bias. Slice selection further introduces opportunity for bias; the process is influenced by the researcher's ability to distinguish fiber directions and position within the vessel wall. More detailed figures demonstrating vessel features and CHP expression have been included in the provided supplemental data (Figures S1-S5) to further demonstrate how damage may be distributed as fiber direction changes with position in the vessel wall. It would clearly be ideal to develop an automated algorithm of vessel damage to eliminate potential issues with researcher bias. This is an ongoing effort in our laboratory. Although such an approach does not yet exist, the presented results demonstrate obvious visual differences supporting our conclusions and alleviating concerns of bias in the present work.

Analysis of imaged vessels was improved over our previous work via development of a variance-controlled standard for control brightness threshold values (i.e. two standard deviations above the mean). Previous methods relied on arbitrary assessment of perceived damage to determine a threshold value, leading to a potentially more conservative approach. As noted, areas of more subtle damage were often excluded from the final analysis [10]. Moving to an approach based on the distribution of control pixel brightness allows for more sensitivity when detecting damage areas and is more accommodating of inter-specimen differences in controls.

As part of this work, we sought to improve our CHP quantification methodology using the methodology reported by Lin et al. [42], where microplate readings of enzymatically digested tissue provide a global quantification of CHP attachment. However, analysis of digested vessels here resulted in no substantial difference in brightness relative to vessel controls, regardless of rate-dependent grouping. Both controls and damaged vessels, however, were more fluorescent than blanks of pure Proteinase K. Within the context of results found using confocal microscopy, it seems likely that the enzymatic approach described here is not sensitive enough for use with tissue samples of this size (average area of 2.58 mm^2; thickness of roughly 80 μm). While these results do not eliminate the possibility of using this approach for future studies, the size of the target tissue and scale of associated damage should be carefully considered before relying solely on an enzymatic assay. It is also possible that undissolved elastin particulates confounded the assay, as the solution was not filtered prior to microplate analysis, although we saw no remarkable change in emittance following the addition of elastase to the Proteinase K solution.

Normalization is a particular challenge in this method. Weighing samples of this size is generally unreliable outside of a clean room and with commonly available balances, as the average dry weight of the examined vessels was 38.8 μg (max 115.0 μg, min 14.2 μg) and may easily be confounded by dust or other debris introduced during weighing. Similarly, the hydroxyproline assay requires several transfers of liquid, with each transfer potentially contributing to compounding errors. Two-dimensional area is the least likely of the three methods to be affected by error. Obtaining 2-D area via microscopy has the additional benefit of providing microscopy data which may be critical for a full understanding of damage characteristics. Because comparison between all three normalization methods led to little difference between any given method, we recommend using 2-D area. We ultimately conclude that the microplate reader-based method may not be appropriate for small arteries due to the high level of baseline collagen remodeling, low sensitivity of the microplate reader, and the loss of layer-specific analysis due to protease digestion. Researchers should thus

consider using confocal-based imaging for the evaluation of CHP in small tissues and in cases where layer-specific information is important.

4.5. Biologic implications

Preliminary postmortem controlled cortical impact (CCI) studies on sheep in our laboratory (unpublished) showed a lack of CHP binding in cerebral arteries, even in regions immediately proximal to sites of hemorrhage. These in vivo results are consistent with the present in vitro findings; that is, high-rate failure does not appear to lead to substantial tropocollagen denaturation. Because of this decreased amount of denaturation, identification of tropocollagen denaturation may have limited value in the description of cerebral vessel damage following TBI.

Other potential implications of the observed rate dependence of molecular damage include the effect that rate may have on healing, or on remodeling subsequent to injury. Veres et al. found that macrophage-like cells (U937) behave differently when seeded on fibrils damaged by overstretch than they do on matched controls [56]; specifically, they reported U937-induced enzymatic digestion in locations of denatured tropocollagen [57]. Given this association between denatured collagen and healing response, a substantial decrease in molecular denaturation during tissue damage may elicit a weaker biologic response to the injury. Rate may then be a useful parameter to change the healing response following procedures such as angioplasty or surgical incision. Likewise, other vascular interventions may be better informed by a more complete damage model considering rate as an important factor in collagen damage levels.

Disclosures

The authors declare the following competing financial interest: Dr. S.M.Y. is a cofounder of 3Helix which commercializes the collagen hybridizing peptides. No other authors have conflicting interests to disclose.

Declaration of Competing Interest

The authors declare the following financial interests/personal relationships which may be considered as potential competing interests: The authors declare the following competing financial interest(s): Dr. S.M.Y. is a cofounder of 3Helix which commercializes the collagen hybridizing peptides.

Acknowledgements

The Henry M. Jackson Foundation for the Advancement of Military Medicine (HJF), partially funded by the U.S. Army Medical Research and Development Command (Contract No. W81XWH-17-2-0008).

National Science Foundation (NSF) (Award No. 2027367).

We acknowledge Cell Imaging Core at the University of Utah for use of equipment.

Supplementary materials

Supplementary material associated with this article can be found, in the online version, at doi:10.1016/j.actbio.2023.04.032.

References

[1] K. Kenney, F. Amyot, M. Haber, A. Pronger, T. Bogoslovsky, C. Moore, R. Diaz-Arrastia, Cerebral vascular injury in traumatic brain injury, Exp. Neurol. 275 (Pt 3) (2016) 353–366.
[2] K.L. Monson, M.I. Converse, G.T. Manley, Cerebral blood vessel damage in traumatic brain injury, Clin. Biomech. 64 (2019) 98–113.
[3] C.L. Zollikofer, E. Salomonowitz, R. Sibley, J. Chain, W.F. Bruehlmann, W.R. Castaneda-Zuniga, K. Amplatz, Transluminal angioplasty evaluated by electron microscopy, Radiol 153 (2) (1984) 369–374.
[4] S. Sherifova, G.A. Holzapfel, Biomechanics of aortic wall failure with a focus on dissection and aneurysm: a review, Acta Biomater. 99 (2019) 1–17.
[5] Y. Kawamura, S.I. Murtada, F. Gao, X. Liu, G. Tellides, J.D. Humphrey, Adventitial remodeling protects against aortic rupture following late smooth muscle-specific disruption of TGFbeta signaling, J. Mech. Behav. Biomed. Mater. 116 (2021) 104264.
[6] E.D. Bell, J.W. Sullivan, K.L. Monson, Subfailure overstretch induces persistent changes in the passive mechanical response of cerebral arteries, Front. Bioeng. Biotechnol. 3 (2) (2015) 2.
[7] W.R. Castaneda-Zuniga, A. Formanek, M. Tadavarthy, Z. Vlodaver, J.E. Edwards, C. Zollikofer, K. Amplatz, The mechanism of balloon angioplasty, Radiolology 135 (3) (1980) 565–571.
[8] H. Weisbecker, D.M. Pierce, P. Regitnig, G.A. Holzapfel, Layer-specific damage experiments and modeling of human thoracic and abdominal aortas with non-atherosclerotic intimal thickening, J. Mech. Behav. Biomed. Mater. 12 (2012) 93–106.
[9] N. Austin, L.M. DiFrancesco, W. Herzog, Microstructural damage in arterial tissue exposed to repeated tensile strains, J. Manipulative Physiol. Ther. 33 (1) (2010) 14–19.
[10] M.I. Converse, R.G. Walther, J.T. Ingram, Y. Li, S.M. Yu, K.L. Monson, Detection and characterization of molecular-level collagen damage in overstretched cerebral arteries, Acta Biomater. 67 (2018) 307–318.
[11] E. Maher, M. Early, A. Creane, C. Lally, D.J. Kelly, Site specific inelasticity of arterial tissue, J. Biomech. 45 (8) (2012) 1393–1399.
[12] E.D. Bell, J.W. Sullivan, K.L. Monson, Subfailure overstretch induces persistent changes in the passive mechanical response of cerebral arteries, Front. Bioeng. Biotechnol. 3 (2015) 2.
[13] T.C. Gasser, Damage in vascular tissues and its modeling, in: Material Parameter Identification and Inverse Problems in Soft Tissue Biomechanics, 2017, pp. 85–118.
[14] J.M. Mattson, R. Turcotte, Y. Zhang, Glycosaminoglycans contribute to extracellular matrix fiber recruitment and arterial wall mechanics, Biomech. Model. Mechanobiol. 16 (1) (2017) 213–225.
[15] M. Ghasemi, D.R. Nolan, C. Lally, An investigation into the role of different constituents in damage accumulation in arterial tissue and constitutive model development, Biomech. Model. Mechanobiol. 17 (6) (2018) 1757–1769.
[16] H. Weisbecker, C. Viertler, D.M. Pierce, G.A. Holzapfel, The role of elastin and collagen in the softening behavior of the human thoracic aortic media, J. Biomech. 46 (11) (2013) 1859–1865.
[17] M. Marino, M.I. Converse, K.L. Monson, P. Wriggers, Molecular-level collagen damage explains softening and failure of arterial tissues: a quantitative interpretation of CHP data with a novel elasto-damage model, J. Mech. Behav. Biomed. Mater. 97 (2019) 254–271.
[18] M.R. Bersi, C. Bellini, J.D. Humphrey, S. Avril, Local variations in material and structural properties characterize murine thoracic aortic aneurysm mechanics, Biomech. Model. Mechanobiol. 18 (1) (2019) 203–218.
[19] J.D. Chalupnik, C.H. Daly, H.C. Merchant, Material Properties of Cerebral Blood Vessels, Univ. of Washington, Seattle, 1971 Final Report on Contract No. NIH-69-2232.
[20] M.C. Lee, R.C. Haut, Strain rate effects on tensile failure properties of the common carotid artery and jugular veins of ferrets, J. Biomech. 25 (8) (1992) 925–927.
[21] K.L. Monson, W. Goldsmith, N.M. Barbaro, G.T. Manley, Axial mechanical properties of fresh human cerebral blood vessels, J. Biomech. Eng. 125 (2) (2003) 288–294.
[22] R.W. Lawton, Measurements on the elasticity and damping of isolated aortic strips of the dog, Circulation Res. 3 (4) (1955) 403–408.
[23] R. Collins, W.C.L. Hu, Dynamic deformation experiments on aortic tissue, J. Biomech. 5 (4) (1972) 333-334, 335–337.
[24] B.D. Stemper, N. Yoganandan, F.A. Pintar, Mechanics of arterial subfailure with increasing loading rate, J. Biomech. 40 (8) (2007) 1806–1812.
[25] E.D. Bell, M. Converse, H. Mao, G. Unnikrishnan, J. Reifman, K.L. Monson, Material properties of rat middle cerebral arteries at high strain rates, J. Biomech. Eng. 140 (7) (2018) 071004.
[26] N. Pearson, G.M. Boiczyk, V.B. Kote, A. Sundaramurthy, D.R. Subramaniam, J.E. Rubio, G. Unnikrishnan, J. Reifman, K. Monson, A strain rate-dependent constitutive model for gottingen minipig cerebral arteries, J. Biomech. Eng. 144 (8) (2022).
[27] T.L. Willett, R.S. Labow, N.C. Avery, J.M. Lee, Increased proteolysis of collagen in an in vitro tensile overload tendon model, Ann. Biomed. Eng. 35 (11) (2007) 1961–1972.
[28] N.C. Chambers, T.W. Herod, S.P. Veres, Ultrastructure of tendon rupture depends on strain rate and tendon type, J. Orthop. Res. 36 (11) (2018) 2842–2850.
[29] Wess, T.J., 2008, “Collagen Fibrillar Structure and Hierarchies,” Collagen, P. Fratzl, ed., Springer US, pp. 49–80.
[30] Eyre, D.R., and Wu, J.-J., 2005, “Collagen Cross-Links,” Collagen, B. J., H. Notbohm, and P. K. Müller, eds., Springer, Berlin, pp. 207–229.
[31] K.A. Piez, Cross-linking of collagen and elastin, Annu. Rev. Biochem. 37 (1) (1968) 547–570.

[32] Y. Li, C.A. Foss, D.D. Summerfield, J.J. Doyle, C.M. Torok, H.C. Dietz, M.G. Pomper, S.M. Yu, Targeting collagen strands by photo-triggered triple-helix hybridization, Proc. Natl. Acad. Sci. U. S. A. 109 (37) (2012) 14767–14772.
[33] J. Hwang, Y. Huang, T.J. Burwell, N.C. Peterson, J. Connor, S.J. Weiss, S.M. Yu, Y. Li, In situ imaging of tissue remodeling with collagen hybridizing peptides, ACS Nano 11 (10) (2017) 9825–9835.
[34] J.L. Zitnay, Y. Li, Z. Qin, B.H. San, B. Depalle, S.P. Reese, M.J. Buehler, S.M. Yu, J.A. Weiss, Molecular level detection and localization of mechanical damage in collagen enabled by collagen hybridizing peptides, Nat. Commun. 8 (2017) 14913.
[35] S.E. Szczesny, C. Aeppli, A. David, R.L. Mauck, Fatigue loading of tendon results in collagen kinking and denaturation but does not change local tissue mechanics, J. Biomech. 71 (2018) 251–256.
[36] J.L. Zitnay, G.S. Jung, A.H. Lin, Z. Qin, Y. Li, S.M. Yu, M.J. Buehler, J.A. Weiss, Accumulation of collagen molecular unfolding is the mechanism of cyclic fatigue damage and failure in collagenous tissues, Sci. Adv. 6 (35) (2020) eaba2795.
[37] J.L. Zitnay, A.H. Lin, J.A. Weiss, Tendons exhibit greater resistance to tissue and molecular-level damage with increasing strain rate during cyclic fatigue, Acta Biomater. 134 (2021) 435–442.
[38] A.H. Lin, A.N. Allan, J.L. Zitnay, J.L. Kessler, S.M. Yu, J.A. Weiss, Collagen denaturation is initiated upon tissue yield in both positional and energy-storing tendons, Acta Biomater. 118 (2020) 153–160.
[39] H. Bastien, A. Bouamoul, D. Rancourt, Soft Tissue Strain Rates in Side-Blast Incidents, Defence Research and Development Canada, Valcartier Research Centre, Quebec City, 2014.
[40] L. Zhang, R. Makwana, S. Sharma, Brain response to primary blast wave using validated finite element models of human head and advanced combat helmet, Front. Neurol. (2013) 4.
[41] H.W. Weizsacker, H. Lambert, K. Pascale, Analysis of the passive mechanical properties of rat carotid arteries, J. Biomech. 16 (9) (1983) 703–715.
[42] A.H. Lin, J.L. Zitnay, Y. Li, S.M. Yu, J.A. Weiss, Microplate assay for denatured collagen using collagen hybridizing peptides, J. Orthop. Res. 37 (2) (2019) 431–438.
[43] S. Brown, M. Worsfold, C. Sharp, Microplate assay for the measurement of hydroxyproline in acid-hydrolyzed tissue samples, BioTechniques 30 (1) (2001) 38–42.
[44] T.L. Willett, R.S. Labow, J.M. Lee, Mechanical overload decreases the thermal stability of collagen in an in vitro tensile overload tendon model, J. Orthop. Res. 26 (12) (2008) 1605–1610.
[45] J.E. Scott, Elasticity in extracellular matrix 'shape modules' of tendon, cartilage, etc. A sliding proteoglycan-filament model, J. Physiol. 553 (Pt 2) (2003) 335–343.
[46] T. Christian Gasser, An irreversible constitutive model for fibrous soft biological tissue: a 3-D microfiber approach with demonstrative application to abdominal aortic aneurysms, Acta Biomater. 7 (6) (2011) 2457–2466.
[47] Puxkandl, R., Zizak, I., Paris, O., Keckes, J., Tesch, W., Bernstorff, S., Purslow, P., and Fratzl, P., 2002, "Viscoelastic properties of collagen: synchrotron radiation investigations and structural model," 357(1418), pp. 191–197.
[48] H. Kahn, R. Ballarini, Steven, Viscoelastic properties of isolated collagen fibrils, Biophys. J. 100 (12) (2011) 3008–3015.
[49] T.J. Bonner, N. Newell, A. Karunaratne, A.D. Pullen, A.A. Amis, M.J.B. A, S.D. Masouros, Strain-rate sensitivity of the lateral collateral ligament of the knee, J. Mech. Behav. Biomed. Mater. 41 (2015) 261–270.
[50] P.B. Canham, E.A. Talman, H.M. Finlay, J.G. Dixon, Medial collagen organization in human arteries of the heart and brain by polarized light microscopy, Connect. Tissue Res. 26 (1–2) (1991) 121–134.
[51] B.K. Wicker, H.P. Hutchens, Q. Wu, A.T. Yeh, J.D. Humphrey, Normal basilar artery structure and biaxial mechanical behaviour, Comput. Methods Biomech. Biomed. Eng. 11 (5) (2008) 539–551.
[52] P. Kannus, Structure of the tendon connective tissue, Scand. J. Med. Sci. Sports 10 (6) (2000) 312–320.
[53] M.I. Converse, K.L. Monson, Biaxial softening of isolated cerebral arteries following axial overstretch, J. Mech. Behav. Biomed. Mater. 118 (2021) 104447.
[54] D. Balzani, S. Brinkhues, G.A. Holzapfel, Constitutive framework for the modeling of damage in collagenous soft tissues with application to arterial walls, Comput. Method Appl. M. 213 (2012) 139–151.
[55] G.A. Holzapfel, R.W. Ogden, A damage model for collagen fibres with an application to collagenous soft tissues, Proc. Math. Phys. Eng. Sci. 476 (2236) (2020) 20190821.
[56] S.P. Veres, E.P. Brennan-Pierce, J.M. Lee, Macrophage-like U937 cells recognize collagen fibrils with strain-induced discrete plasticity damage, J. Biomed. Mater. Res. A 103 (1) (2015) 397–408.
[57] S.P. Veres, J.M. Lee, Designed to fail: a novel mode of collagen fibril disruption and its relevance to tissue toughness, Biophys. J. 102 (12) (2012) 2876–2884.